Discharge of hydrothermal fluids through sediment at the Escanaba Trough, Gorda Ridge (ODP Leg 169): assessing the effects on the rock magnetic signal

Michael Urbat [a],*, Mark J. Dekkers [b], Klaus Krumsiek [a]

[a] *Department of Geology, University of Cologne, Zülpicher Strasse 49a, 50674 Cologne, Germany*
[b] *Paleomagnetic Laboratory 'Fort Hoofddijk', Faculty of Earth Sciences, Utrecht University, Budapestlaan 17, 3584 CD Utrecht, The Netherlands*

Abstract

An integrated rock-magnetic and multivariate statistical analysis of a suite of sediment samples recovered from ODP Sites 1037 and 1038 (Leg 169, Escanaba Trough, Gorda Ridge spreading center, NE Pacific Ocean) has been carried out to assess the use of the sediment magnetic signal as a tracer of post-depositional alteration related to the discharge of hydrothermal fluids through these sediments. The uppermost (above 40 mbsf) section of three separate holes (Holes 1037 B, 1038 I and 1038 G) was sampled; previous sedimentological and geochemical studies indicated that these holes represent a transect from unaltered to strongly hydrothermally influenced sediments. Analysis of NRM, ARM, anisotropy of magnetic susceptibility (AMS), hysteresis parameters and low-temperature magnetic properties suggest increasing alteration of the magnetic minerals with increasing circulation of hydrothermal circulation of fluids. Fuzzy *c*-means clustering combined with non-linear mapping yields a more elaborate picture because similar alteration groupings at different holes can be compared. At Hole 1037 B, a sedimentary reference site drilled away from the area of high heat flow, the rock-magnetic signal is a sensitive record of changes in detrital inputs. Magnetite and some monoclinic pyrrhotite are detected. The detrital magnetic signal is still apparent at intermediate Hole 1038 I, but cluster analysis detects an increasing hydrothermal influence on the magnetomineralogy in the lower part of the hole. Strong hydrothermal alteration at Hole 1038 G results in a complete loss of the detrital/diagenetic magnetic signal, which is replaced by a much weaker 'hydrothermal' signal composed of monoclinic pyrrhotite and pyrite. The alteration of the magnetic signal is not restricted to the uppermost few meters of the sediment column and the magnetic properties of the sediment can be used to trace even minor alterations of marine sediments related to the lateral and vertical advection of hydrothermal fluids which may easily be overlooked by more traditional methods. © 2000 Elsevier Science B.V. All rights reserved.

Keywords: remanent magnetization; multivariate analysis; Escanaba Trough; hydrothermal conditions; ODP Site 1037; ODP Site 1038

1. Introduction

The magnetic signal in marine sediments is a combination of several components with a varia-

* Corresponding author. Tel.: +49-221-470-6584; Fax: +49-221-470-5149; E-mail: m.urbat@uni-koeln.de

ble genetic origin. Commonly, a detrital suite of magnetic minerals undergoes some (early) diagenetic alteration as a function of sediment depth due to increasingly reducing conditions (e.g. [1]), involving dissolution of magnetite (e.g. [2]) and/or new formation of magnetic minerals, particularly sulfides (e.g. [3,4]). The extent of diagenetic overprint on the natural remanent magnetization (NRM) ranges from (virtually) absent to (nearly) complete. Clearly, the degree of masking of the original detrital remanent magnetization must be established for a proper magnetostratigraphic or paleoclimatic interpretation of a sediment column. Magnetic minerals, occurring in trace amounts in sediments, can record minute changes in the geochemical environment and, therefore, the sensitive mineral-magnetic techniques may have the potential to reveal incipient alteration processes that otherwise go unnoticed.

Here, we present a mineral-magnetic study of the sediments of Escanaba Trough, which are variably affected by diffuse discharge of hydrothermal fluids [5]. During Leg 169 on board R/V *JOIDES Resolution*, magnetic susceptibility was successfully used to recognize individual turbiditic layers in the sediment column. Also, a complete removal of the magnetic signal as a function of the hydrothermal circulation was suspected [6]. To arrive at a better understanding of the subtleties contained in the mineral-magnetic signal, the behavior of individual magnetic parameters served as a basis for a joint interpretation of all parameters using multivariate statistical techniques. Fuzzy *c*-means clustering (FCM) and non-linear mapping (NLM) were used to identify groups within the data that could be assigned environmental and sedimentological significance.

2. Geological background

The Gorda Ridge off-coast of Oregon and northern California is offset by the transcurrent fault systems of the Blanco Fracture Zone in the North and the Mendocino Fracture Zone in the South [7] (Fig. 1). The morphology of the slow-spreading ridge is characterized by an axial valley that lies at a waterdepth of > 3250 m. The Esca-

naba Trough forms the southernmost part of the Gorda Ridge. The valley is flanked by steep, 900–1500 m high, walls and widens from 10 to ca. 18 km at the southern end where it is covered by > 900 m interbedded hemipelagic and turbiditic sediments. The Ocean Drilling Program (ODP) Leg 169 Sites 1037 and 1038 are located at Central Hill (40°06′N, 127°29.56′W; Fig. 1), one of the numerous small sediment hills that result from volcanic and intrusive emplacement of ridge axis basalts. The hill is 1 km in diameter, 60 m high and has steep sides. The western part of Central Hill contains the most extensive sulfide deposits observed in the Escanaba Trough and is actively venting high-temperature hydrothermal
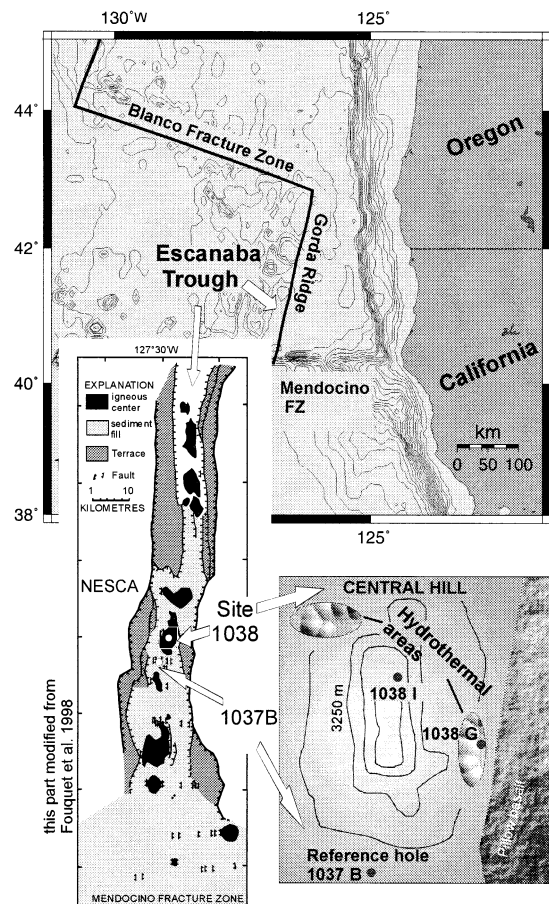

Fig. 1. Location map.

fluids. The chemical composition of these fluids is substantially different from mid-ocean ridge (MOR) hot springs due to their interaction with the overlying sediment [8]. The southeast side of the hill, investigated in this study, issues diffuse, presumably low-temperature fluid from a small mound. In this area, sulfide mineralization and vent-specific fauna was observed during submersible dives [9]. Accordingly, sediments in the vicinity of the Hill are low to highly altered, pertaining to diagenesis, hydrothermal circulation, basalt intrusion and sulfide mineralization, one of the subjects of the ODP Leg 169 cruise.

The turbiditic sediment fill at Escanaba Trough originates from the Columbia River (latitude 46.2°N) several hundreds of kilometers to the North of the drilling sites; a hyperpycnal flow entering Escanaba Trough from the South is proposed as the likely transport mechanism [10]. Since the underlying crust is very young [11] and because sedimentation rates during the Holocene are very high [10,12], most of the sediment fill was probably accumulated during the last two or three Pleistocene sea-level low-stands. Accelerator mass spectrometry ^{14}C dates indicate an age of 116 kyr at 21.57 mbsf at Hole 1037 B; average sedimentation rates for the turbiditic intervals are calculated to be ∼13.8 m/kyr in contrast to ∼0.17 m/kyr for the hemipelagic intervals [10].

3. Holes and sample material

Ocean Drilling Program Leg 169 drilled a transect of holes in the vicinity of Central Hill (Holes 1038 A to I [7]). The present rock-magnetic study addresses the uppermost 40 m of Holes 1038 I (on top of the hill; Fig. 1), 1038 G (southeastern part with diffuse discharge at low temperatures) and the upper section of sedimentary Reference Hole 1037 B. This hole was drilled away from hydrothermal venting in the Escanaba Trough [7] and provides the sedimentary/rock magnetic background to the study. Shipboard visual core description and smear slide analysis recognize two alteration facies A and B [6]. Alteration facies A is defined as relatively unaltered primary sediment. Facies B is characterized by

authigenic carbonate in the form of cement or carbonate nodules which is taken to indicate thermally-accelerated rates of diagenesis. Geochemical analyses of pore fluids also identify gradients in the degree of alteration between the holes [6]. Levels of ammonia (produced during the oxidation of organic material) increase between 1037 B (0.5–2.8 mM) to 1038 I (0.1–4.5 mM) to 1038 G (7.6–7.8 mM). These data suggest progressively increasing rates of diagenesis, which is probably thermally driven, providing that the sediment composition (e.g. organic carbon content) and the sedimentation rates do not vary markedly between the holes. The temperature gradient in 1037 B is 0.15°C m^{-1}, compared to an estimated gradient of 2°C m^{-1} in 1038 I (55.7°C at 26.8 mbsf [6]). No temperature records are available for 1038 G, but analyses of hydrocarbon gases trapped within the sediment indicates that they are thermogenic and formed at temperatures between 200–300°C. In addition, the exceptionally high Cl content of the pore fluids recovered from between 0–40 mbsf in this hole (679–776 mM [6]) relative to local bottom seawater (560 mM) indicates that the pore fluids must be derived from hydrothermal circulation that has extended into basement oceanic crust (rather than through the involvement of hydrous mineral phases or interaction with sediment-hosted sill complexes [5]).

Recovery permitting, 6 cm^3 cubic samples were taken quasi-continuously at about every 15 cm. Generally, the sediment is composed of well-sorted sand and silt interbedded with clay, clayey silt and silty clay. One hundred samples, all alteration facies A, were taken from the Reference Hole 1037 B (cores 1H1 to 3H5, 0.19–23.44 mbsf). Sixty samples were collected from Hole 1038 I (cores 1X1 to 4H6, 0.47–34.88 mbsf). Samples from the interval 0–26.8 mbsf are assigned to alteration facies A; below this depth samples are assigned to alteration facies B. Sixty samples collected from Hole 1038 G (cores 3H1 to 4H8, 22.17–41.33 mbsf) are all assigned to alteration facies B. Note, that three gaps in the sediment column at Hole 1038 I (Fig. 6) result from 0% core recovery and an interval of drilling related lateral inflow of material (lowermost gap). There

was no core recovery between 0–22 mbsf in Hole 1038 G [7].

4. Methods and instrumentation

Magnetic measurements were carried out at the paleomagnetic laboratory 'Fort Hoofddijk' (Utrecht University, The Netherlands). NRM intensities were measured on a three-axis 2G DC-SQUID magnetometer (noise level 5×10^{-12} Am^2). Three-axis static alternating field (AF) demagnetization up to 70 mT was used to determine the characteristic remanent magnetization (ChRM). Volume susceptibilities (κ) and anisotropy of magnetic susceptibility (AMS) were measured at room temperature on a KLY-2 susceptibility bridge (noise level 4×10^{-8} SI; AGICO, Czech Republic). Anhysteretic remanent magnetization (ARM) was imparted perpendicular to the bedding plane (150 mT peak AF; 29.5 µT dc bias field parallel to AF). Pilot samples with varying peak AFs showed that ARM intensity after 150 mT peak AF can be regarded as the maximum ARM that can be imparted in the samples.

Thermomagnetic and hysteresis measurements were carried out on previously dried and weighed subsamples (typically ~ 0.07 g). Thermomagnetic measurements were performed as repeated heating/cooling cycles to increasingly elevated temperatures up to 700°C using a modified horizontal translation Curie balance ([13]; noise level 2×10^{-9} Am^2). Hysteresis measurements were carried out at room temperature on an alternating gradient magnetometer (AGM), Micromag 2900 (Princeton Measurements Corporation, USA; noise level $\sim 10^{-11}$ Am^2). Maximum fields used were 2 T. The coercivity of remanent magnetization B_{cr} was also determined using the Micromag 2900, as were the low-temperature (LT) remanence measurements. At room temperature a 1.6 T field is given and the sample is subsequently cooled down to about 20 K using liquid helium.

We employed FCM clustering using the algorithm and program of [14] combined with NLM according to the lines set out in [15]. A more elaborate consideration of the statistical methodology, its advantages, potential applications and pitfalls focusing on the mineral-magnetic analysis of marine sediments is described in [16]. Examples of successful application of this methodology are [16–20].

5. Results

5.1. Behavior of NRM and mineral-magnetic parameters

NRM demagnetization diagrams show univectorial decay to the origin. No excursional directions are found in the samples and all directions conform to the expected mean value of the geocentric axial dipole for the site. Demagnetization at 20 mT AF removes viscous and possible drilling-induced components. For the alteration facies A samples, the lowest intensities (10–20 mAm^{-1}) are recorded in the hemipelagic sediment at the top of the sediment column (Fig. 2). Intensities in the sandy turbiditic layers vary between 30 and 100 mAm^{-1}, with occasional values to over 200 mAm^{-1}. Alteration facies A samples of Hole 1038 I have more constant NRM intensities of ca. 100 mAm^{-1}. Facies B samples have slightly lower NRM intensities of ca. 70–80 mAm^{-1}. Note, that below 19 mbsf samples from Hole 1038 I display a much stronger loss of magnetization intensity between 0 and 20 mT (not shown). In Hole 1038 G intensities (facies B) are ca. 20 mAm^{-1} for the top 31 m of the core and the AF-demagnetization is similar to the lower part of hole 1038 I. Below 31 mbsf values drop by almost an order of magnitude to ca. 3 mAm^{-1}.

Volume susceptibility κ at reference Hole 1037 B spans more than one order of magnitude ranging from ca. 300–7000 µSI (Fig. 2). κ appears to re-

$\rightarrow$

Fig. 2. Downhole plots of mineral-magnetic parameters for Holes 1037b (a), 1038I (b) and 1038G (c). Refer to Fig. 9 for symbol coding indicating the FCM cluster results. T, base of a turbiditic interval; H, hemipelagite. Note differences in depth-scale.
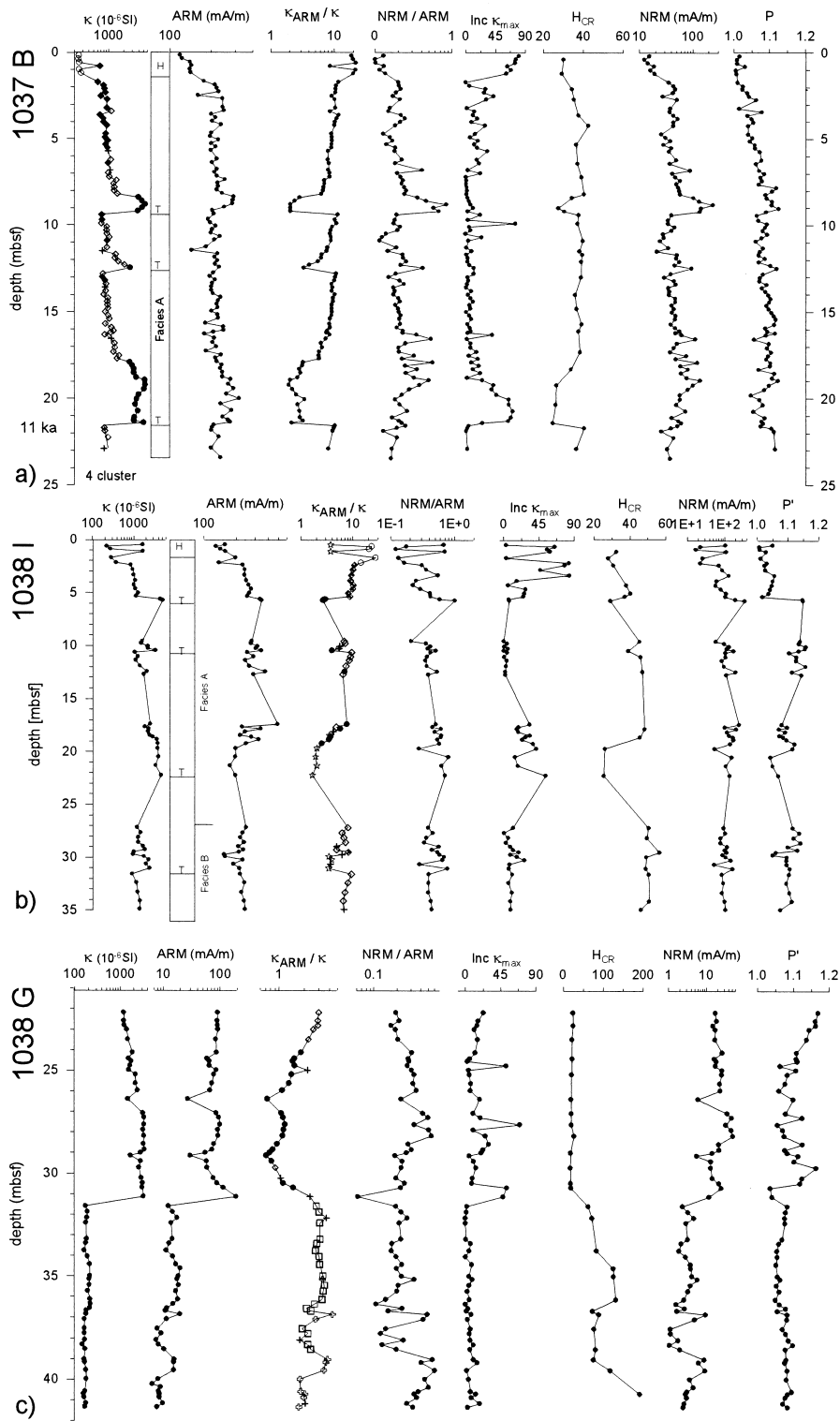
flect (primary) lithological variations. The hemipelagic sediments have the lowest κ, the three fining-upward turbidites have values from 800 μSI upward with the highest values for the more sandy bases (Fig. 2a). Alteration facies A samples in Hole 1038 I show less variation in κ values, gradually increasing with depth from ca. 1000 to ca. 3000 μSI. Facies B samples have values of ca. 1000 μSI (Fig. 2b). The upper 31 m of Hole 1038 G show increasing κ values from 1000 μSI to ca. 3000 μSI before abruptly plunging to ca. 200 μSI further down (Fig. 2c). There is no apparent lithological change at this depth [6].

The degree of anisotropy, P' [28], is surprisingly high for marine sediments and ranges from 1.00 to 1.15. We suspect that this is related to the contribution of a highly anisotropic mineral like pyrrhotite [29] to the magnetic signal. In the upper 7 m of the sediment column in Hole 1037 B P' gradually increases to ca. 1.10. In Hole 1038 I the top 5 m has low P' values at ca. 1.05, deeper down P' values are 1.10–1.15 regardless of alteration facies A or B. In Hole 1038 G the upper 31 m show variable and high P' values, the lower half of the core has more constant P' values.

The long axes of the anisotropy ellipsoid (Incκ_{max}) are predominantly in the horizontal plane (Incκ_{max} = 0) indicating an undisturbed sediment fabric. Incκ_{max} deviates significantly from horizontal in the hemipelagic sediment, presumably because of the poor consolidation of these topmost sediments, as well as in the sandy layers. The latter may be due to a less well developed adsorption of the magnetic carriers on platty clay minerals in the sandy intervals. In the upper 7 m of the sediment in Hole 1037 B Incκ_{max} values are more commonly around 20° concomitant with a continuous decrease of P' towards lowest values at the top of the sediment column.

Anhysteretic remanent magnetization ARM (Fig. 2) mimics the general downhole behavior of κ and NRM in all three holes. The intensities, however, have a more restricted range (100–300 mAm^{-1}). In the lower half of Hole 1038 G, below 31 mbsf, ARM intensities vary between 10 and 20 mAm^{-1}. A bivariate plot of κ versu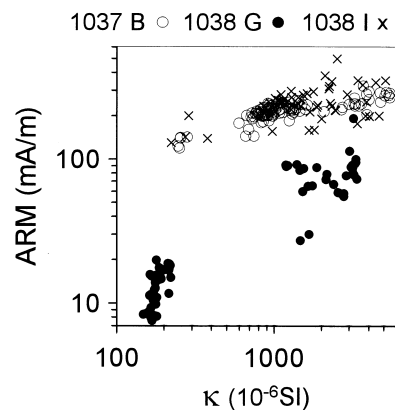s ARM (or M_{rs}) indicates that linear correlation in samples from Hole 1037 B is poor ($R^2 = 0.5$) and even absent at the highest susceptibility values (Fig. 3; sandy base of the turbidites). In samples from Hole 1038 I there is no correlation of ARM with κ throughout the sampled interval. Samples from Hole 1038 G form two groups and plot to the left of the samples from the other two holes. At the highest susceptibility values (>2000 μSI) the influence from clay minerals on κ is insignificant. Shifts in relative amounts of remanence carrying minerals could partly explain the differences seen between the holes, because ARM intensities will be affected more than κ. ARM preferentially magnetizes finer magnetic grains and the ratio NRM/ARM (Fig. 2) is a measure of the relative amount of finer grains contributing to NRM. The ratio can give information on the alignment efficiency of the NRM if the grain-size distribution in the various lithologies is comparable. The NRM$_{@\ 20\ mT}$ is about 10% of ARM intensity in the hemipelagic sediment, commonly around 20% in the clays and reaches almost 100% in the sands.

The ratio of the anhysteretic magnetic susceptibility κ_{ARM}/κ mirrors main trends in κ. κ_{ARM}/κ is indicative of relative grain-size changes (lower ratio = coarser grain size) only if the magnetic signal is driven by magnetite. Here, the ratio seems to be influenced by varying relative contributions from remanence carrying minerals to the signal. Ratios are highest in the hemipelagites, within turbiditic sediments they are lower and decrease gradually

Fig. 3. Scatterplot of κ versus ARM intensity summarizing Holes 1037 B, 1038 I and 1038 G.

towards the base of a turbidite where they drop abruptly (Fig. 2). At Hole 1038 G ratios are lowest but show an abrupt increase at 31 mbsf to values of ca. 3 (Fig. 2c).

In Hole 1037 B, B_{cr} is lowest, ca. 25 mT, in the sandy parts of the turbidites. In this core, the hemipelagites have B_{cr} values of ca. 30 mT and the silty/clayey parts of the turbiditic packages have values of ca. 40 mT. B_{cr} values of alteration A facies samples from Hole 1038I range from 25 to 50 mT with no obvious downhole trend. B_{cr} values of facies B samples are ca. 55 mT. At Hole 1038 G, the upper 9 m have low B_{cr} values of ca. 20–25 mT, the lower 10 m have the highest B_{cr} values of the whole data set: from 80–90 mT up to 130–140 mT and occasionally over 200 mT.

5.2. Magnetic mineralogy

Thermomagnetic measurements indicate magnetite by its Curie temperature at ca. 580°C (Fig. 4a–c). It (partially) oxidizes (thermomagnetic runs in air) during heating above 600°C leading to irreversible cooling curves. The Verwey transition at ca. 117 K observed during the LT remanence measurements (Fig. 5) indicates that the original magnetite is pure and non-oxidized (cf. [21]). There is a sharp intensity drop in magnetization intensity at 34 K suggesting pyrrhotite [22]. Maghemite and greigite show flat SIRM cooling curves incompatible with the present observations [23,24]. In the sample of Hole 1037 B the remanence shows a maximum between 50 and 70 K, which is very unusual for pyrrhotite. This maximum is much less pronounced or has disappeared completely in holes affected by hydrothermal activity, leading to more commonly observed shapes of LT curves [25]. Thermomagnetic analysis shows that the pyrrhotite is altering on heating in air, in contrast to other pyrrhotites which are thermally more stable with respect to heating in air. Synthetic pyrrhotite hydrothermally synthesized and quenched from ca. 200°C to room temperature in < 30 s (hence, comparable to black smoker processes) shows the same thermomagnetic behavior [26].

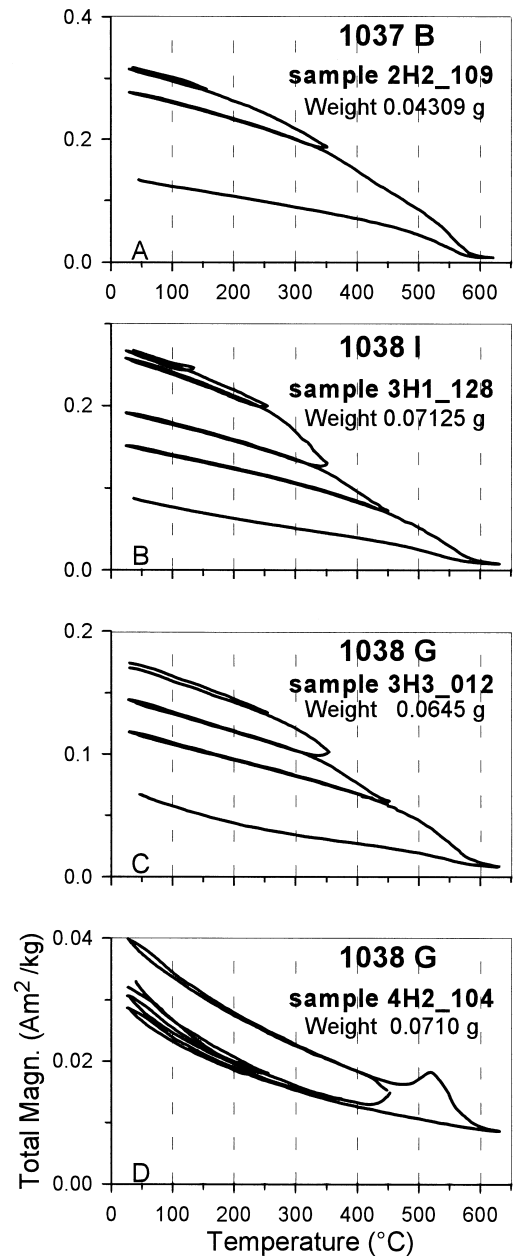The magnetic signal at the reference site Hole 1037 B is dominated by magnetite. Thermomag-

Fig. 4. Thermomagnetic analysis of samples from Hole 1037 B (A), 1038 I (B) and 1038 G (C and D). Note the varying scale of the *y*-axis.

netic runs do not unequivocally confirm the presence of pyrrhotite in samples from the reference site, the low-temperature behavior suggests that it is present. In contrast, samples from Hole 1038 I

show a more distinct drop around 300°C in magnetization in the thermomagnetic runs of the samples than those of Hole 1037 B (Fig. 4a,b). We attribute this to a more prominent contribution from pyrrhotite to the signal in addition to magnetite. Alternative explanations of the thermomagnetic behavior displayed by greigite or maghemite are not compatible with our observations. The rock-magnetic analyses of the upper interval at hole 1038 G above 31 mbsf indicates that the signal is carried dominantly by magnetite and pyrrhotite. The 1038 G low-temperature measurements (Fig. 5) display the most distinct Verwey transition of magnetite when compared to samples from the two other holes. The thermomagnetic runs confirm magnetite and a drop in magnetization around 300°C indicates pyrrhotite. Compared to the 1038 I samples the decrease in magnetization is less prominent and indicates a less significant contribution from pyrrhotite to the magnetic signal. The only magnetic minerals detectable at Hole 1038 G below 31 mbsf are
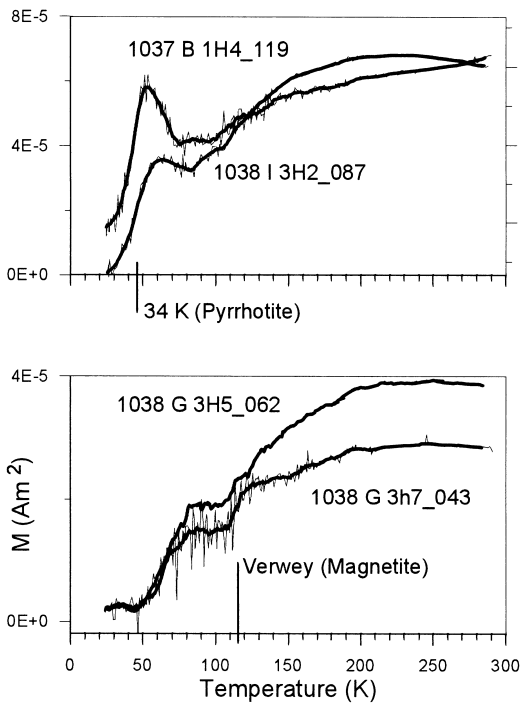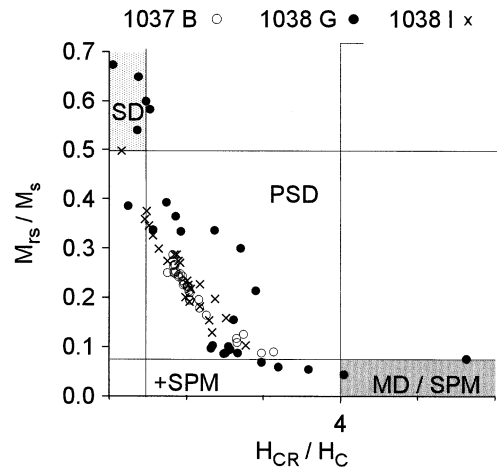

Fig. 6. Day plot for the entire dataset. Note that the plot is not definite indication of domain states due to the mixed mineralogy in all three holes.

pyrite (Fig. 4d) and pyrrhotite. Unfortunately, the LT remanence measurements gave spurious results because of the low magnetization intensities.

Hysteresis behavior indicates that saturation is reached at about 350 mT (not shown). The saturation fields are higher than those expected for magnetite (< 200 mT) and in conjunction with the previous analyses point to the presence of fine-grained SD pyrrhotite, which is magnetically harder than magnetite of the same grain size. Hysteresis loops of 1037 B and 1038 I appear to be very similar throughout the sediment column hinting at only minor changes in grain size or magnetic mineralogy. The samples investigated are magnetically a blend of magnetite and pyrrhotite and, hence, a Day plot [27] cannot be a definite indication of magnetic grain sizes for neither mineral. On a Day plot (Fig. 6), data for Holes 1037 B and 1038 I plot closely together in the same area of the PSD field with the 1038 I samples trending slightly more to the SD area, especially those samples from alteration facies B at hole 1038 I. This could be an indication for an increased pyrrhotite content with respect to the magnetite contribution. The hydrothermally altered Hole 1038 G spreads over the complete band from the SD to the MD fields. Samples from the interval below 31 mbsf where only iron

Fig. 5. Behavior of a room-temperature induced SIRM during cooling to 20 K. Thick lines are the nine-point running average.

sulfides are detected plot in the upper half of the diagram, up to the SD area. This seems to confirm the trend of increasing pyrrhotite contributions noted for hole 1038 I samples. In this interval where intensities drop by one order of magnitude (see above), hysteresis loops are open with high coercivity values pointing to fine-grained SD pyrrhotite (Fig. 6). Magnetite is no longer detectable. The remaining samples from Hole 1038 G plot more to the right than samples from the other sites in the PSD field.

6. FCM and NLM

6.1. Input parameters

From the downhole plots and the scatterplot shown it is evident that the cores show subtle differences. The multiple lithologies and processes are reflected in the mixed magnetic mineralogy and/or grain size, with potentially much overlap among samples. This makes the data set suited for multivariate statistical analysis with a fuzzy logic approach. The following rock-magnetic parameters were included in the FCM and NLM runs: κ, NRM/ARM, κ_{ARM}/κ, P' and ARM. From the initial analysis of the rock-magnetic properties it is clear that none of the parameters used has only one particular meaning with respect to all three holes or individual intervals within a hole. It is important that each parameter employed in the analysis does highlight a different aspect or property of the magnetic signal. The analysis is not jeopardized by changes in the meaning of individual parameters (as long as they have been established previously) and is an expression of the inherently gradual character of post-depositional alterations to the magnetic signal (cf. [16]).

κ at the reference hole, for example, is a measure of the relative concentration of magnetic material in the samples and effectively an indicator of varying detrital inputs. At Hole 1038 G, κ still measures relative concentration variations, however, it is no longer a function of lithology and merely derived from post-depositional alteration of the primary magnetic signal. The same reasoning applies to other parameters. ARM was

chosen because it is, in contrast to κ, only influenced by remanence carrying minerals (dominantly fine-grained magnetite and subordinate pyrrhotite) which react most sensitively to post-depositional processes. κ_{ARM}/κ indicates varying grain sizes in intervals where only magnetite is present, in other intervals it appears to be influenced by the relative ratio of magnetite to pyrrhotite. NRM/ARM measures the alignment efficiency of the finer grained magnetic components. P' is strongly influenced by the concentration of highly anisotropic pyrrhotite in the sediment, because comparatively isotropic magnetite will be swamped.

6.2. Total data set

FCM and NLM in essence show a division in Hole 1038 G and Holes 1037 B and 1038 I. This is what is expected because Holes 1037 B and 1038 I are alike and differ from 1038 G. If the number of clusters is increased finer features of the data set emerge, which roughly conform to the lithological variations at Holes 1037 B and 1038 I and the subdivision into two intervals at Hole 1038 G. Up to a total of seven clusters for the entire data-set FCM results are consistent with NLM, however, no more than the expected major groupings (lithology) are seen. Increasing the number of clusters further, in an attempt to visualize more subtle information leads to distortion of the cluster structure rather than refinement, because fine-tuning at 'one end' distorts the 'other end' of the entire model. Also, the cluster affiliation of individual samples is rather difficult to interpret because samples of different holes are combined in one cluster leading to erratic cluster distributions in downhole plots. One arrives at a comparison of individual samples and comparison of neighboring samples may therefore be difficult. Critically, the total number of clusters required for the entire data set would be too high to conform to a straightforward application of the FCM algorithm. As a rule of thumb, the number of input variables (here five) should not be less than the number of clusters when the data set is not too large [20]. Therefore, we decided to run FCM and NLM on individual holes and for the general in-
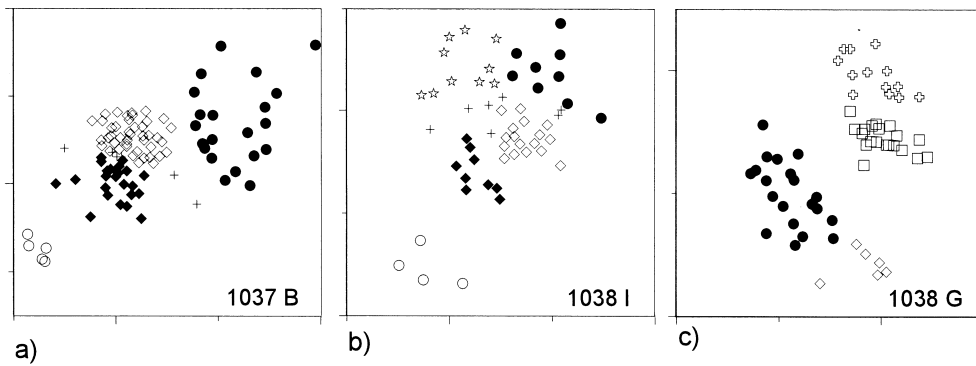
Fig. 7. NLM plots for Holes 1037 B (a), 1038 I (b) and 1038 G (c). Symbol coding indicates FCM results (same as in Fig. 9).

terpretation we compare the meaning of clusters that are alike but not exactly similar.

6.3. FCM analysis of individual holes

6.3.1. Hole 1037 B

From the data displayed in Fig. 5 one would expect at least three (detrital, D) clusters to emerge from Hole 1037 B, on the basis of the generally different rock-magnetic values for the sandy base of the turbidites (cluster DT), the intermediate clay interval (cluster DC) and the hemipelagic sediment (cluster DH). Interestingly, in a four-cluster model the relatively homogeneous clays split into two clusters (cluster DC1 and DC2) consistently throughout the sampled interval. This fourth cluster which we regard as significant (separated clearly in the NLM plots; Fig. 7a), relates to subtle differences in the rock-mag-

netic properties. Using conventional lines of interpretation it is practically impossible to distinguish this grouping. Also, lithological descriptions of the cores [6] do not indicate a consistent grouping in the homogeneous clay zones. Intermediate samples plot coherently downhole between the two clay clusters. This confirms the rather gradual change from cluster DC1 to cluster DC2. Attempts to analyze a higher number of clusters (5–7) results in a loss in the consistency in FCM clustering and NLM analyses indicate over-interpretation (groups start to mingle). Given three distinct sandy turbiditic layers described for the sampled interval of the Reference Site the four cluster model is an appropriate description of three sedimentation events. These are formed from bottom to top by consecutive clusters DT–DC2–DC1. The top of the sediment column is formed by hemipelagic cluster DH.
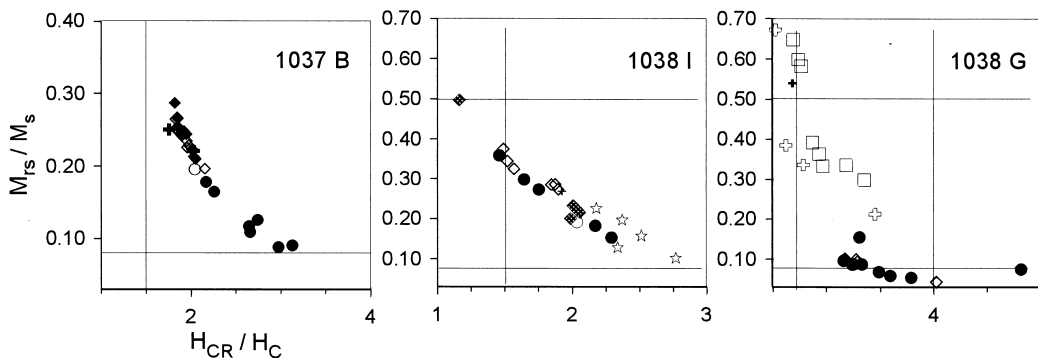

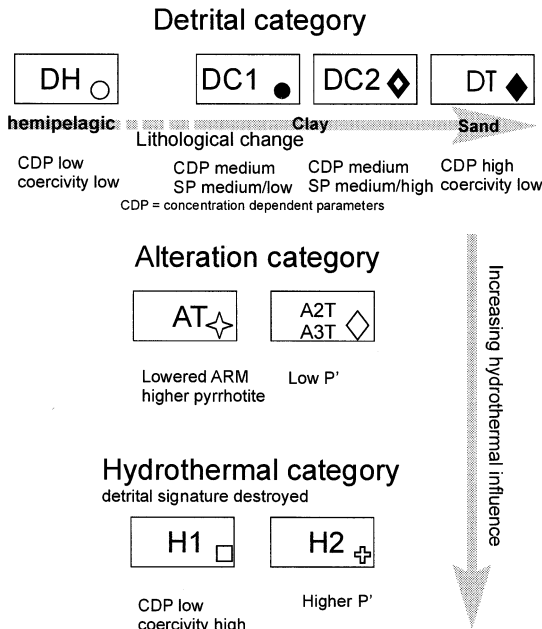Fig. 8. Day plots for the three individual holes with FCM cluster tagging (same as in Fig. 9).

Fig. 9. Summary of the FCM clusters.

6.3.2. Hole 1038 I

FCM indicates that Hole 1038 I is best described by a five-cluster model, confirmed by the corresponding NLM plot (Fig. 7b). The general detrital features are still expressed. The hemipelagic cluster (DH), clusters DC and DT form discrete groupings when plotted downhole. In the lower part of the sediment column (>19 mbsf) an additional cluster emerges in the zone of the DT cluster at the base of a turbidite. This altered turbiditic cluster is labelled AT (Figs. 2b and 7b). Intermediate cases indicate a rather gradual transition between cluster DT and cluster AT.

6.3.3. Hole 1038 G

A four-cluster model best describes the rock-magnetic signal at Hole 1038 G (Figs. 2c and 7c). As for clusters DC1 and DC2 (Hole 1037 B) subtle changes to the rock-magnetic signal discriminate two clusters (cluster A2T and A3T) in the upper part of the sediment column. Two clusters are also identified in the low-intensity zone in the second half of the sediment column (the hydrothermal (H) clusters H1 and H2).

7. Discussion

The cluster affiliation in downhole plots is shown in Fig. 2. The cluster grouping is lithologically consistent per hole. When viewed on a Day plot for each hole with samples labelled according to their cluster affiliation (Fig. 8), however, samples belonging to a single cluster may plot in different places. This indicates that the information contained in the hysteresis parameters is not sufficient to explain all of the observed variance, particularly in Hole 1038 I. A multivariate analysis based on information from all variables is thus superior to scattergram analysis, because more complex information can be visualized.

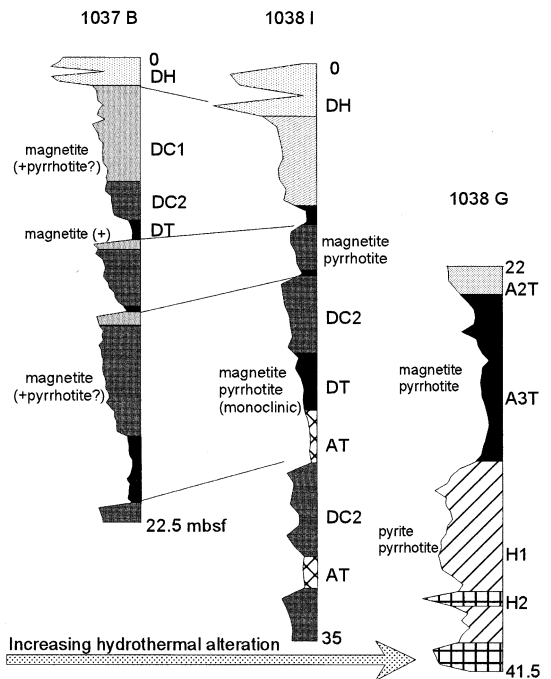Understanding the characteristics of the clusters

Fig. 10. Cartoon of the cluster interpretation over all holes. The gaps in the respective profiles were omitted and the figure is not to scale. A stuffed depth scale more likely is a true representation of the upper interval at Hole 1038 I, especially when the gap resulting from core-flow material is removed. The two gaps above are related to core recovery problems in the more sandy intervals and thus the true thickness is unknown, the general downhole shape of the curve is still maintained. Thin lines indicate a suggested correlation of lithological intervals.

(Fig. 9) is crucial to their interpretation. If we extend the comparison to all available data on the basis of the FCM analyses, it is apparent that those clusters to which we have assigned a common name are not exactly equal. For example, cluster DT occurs in both Hole 1037 B and Hole 1038 I. There are differences between these two DT clusters, but these are marginal compared to differences between the DT clusters and other clusters. Hence, the DT clusters are considered to be equivalent and their meaning can be directly compared. Slight differences amongst similar clusters can also be understood if we consider, for example, that there is no minute correlation of κ and ARM throughout Hole 1038 I, while at Hole 1037 B the linear relation is lost only in the DT clusters. We attribute this to some amount of newly formed fine-grained magnetite affecting ARM more than κ (see above). This component is presumably re-precipitated from Fe^{2+} (previous dissolution of magnetite) and indicates minor diagenetic alteration at those intervals. This magnetite component would then carry a chemical remanent magnetization with a high alignment efficiency, expressed, for example, by the high NRM/ARM ratios in the DT clusters.

Fig. 10 summarizes the rock-magnetic signal at Central Hill as a function of the increasing effect of hydrothermal fluids on the sediment, in the frame of the cluster models derived. At reference Hole 1037 B the magnetic signal appears to sensitively record changes in detrital inputs. Three previously described turbiditic events [6] are confirmed by the rock-magnetic measurements (repetition of cluster sequence DT–DC1–DC2 coherently downhole).

The hemipelagic interval at intermediate Hole 1038 I yields characteristics very similar to those of the reference site (cluster DH). At Hole 1038 I the cluster DC1, equivalent to DC1 just below the hemipelagic sediment at Hole 1037 B, has slightly different characteristics in the top of the core. It completely vanishes at greater depths in the second and third turbiditic interval. Also cluster DT (sandy base of the turbidites) is gradually replaced by cluster AT with increasing depths at Hole 1038 I. This is visible around 19 mbsf where cluster AT forms the lower half of the second turbiditic in-

terval (some meters above the sedimentary boundary between facies A and B). It has entirely replaced cluster DT in the next lithological unit downhole. Clay mineral analyses carried out on Hole 1038 I [30] do not identify clay minerals indicative of hydrothermal processes throughout the sampled interval. The magnetic mineralogy is apparently more sensitive to incipient hydrothermal alteration than the prevailing clay minerals. The more pervasive alteration seen from the rock-magnetic results of the more sandy and hence higher permeable units (clusters DT to AT) suggests that alteration has a lateral component in addition to increasing (temperature accelerated) alteration with depth.

The rock-magnetic clusters emerging from Hole 1038 G do not have common characteristics with Holes 1037 B and 1038 I, apart from some similarities between clusters DT/AT and cluster A3T. The primary magnetic signal has been entirely replaced by pyrite and fine-grained monoclinic pyrrhotite as a consequence of post-depositional alteration. The magnetic signal at Hole 1038 G does not display any detrital features in the second half of the sampled interval starting at 31 mbsf. The transition to a merely hydrothermal magnetic signal at Hole 1038 G is abrupt and appears within a 10–15 cm thick interval. This does not indicate vertical diffusion upwards as there is no prominent lithological change over this interval (see [6]) which would promote such a sharp boundary. If high heatflow alone was responsible for the alteration of the magnetic minerals we would expect a more gradual change in rock-magnetic properties. We therefore suggest that horizontal flow of fluids is involved in the creation of the magnetic signal at Hole 1038 G. The replacement mechanism appears to be driven by the circulation of low to medium temperature fluids under reducing conditions. These reducing conditions probably result from thermally accelerated decomposition of organic matter in the sediment, possibly with some contribution from reactive iron and sulfur in the fluids. Replacement of magnetite via pyrrhotite to pyrite has also been suggested in conjunction with the presence of gas hydrates [31], however, at Escanaba Trough the main driving factor appears to be thermally accelerated diagenesis.

8. Conclusions

Analysis of the rock magnetic properties of sediments recovered from the Escanaba Trough can be used to trace subtle incipient alteration resulting from both lateral and vertical circulation of hydrothermal fluids. Major benefits of this approach are that it is sensitive and it can be analyzed at high resolution. Magnetic minerals are ubiquitous and measurements are relatively fast and comparatively inexpensive. This is further illustrated by the following two examples. Firstly, the magnetic signal in Hole 1038 G identifies a sharp boundary at 31 mbsf consistent with lateral advection of hydrothermal fluids. This boundary was also identified by organic geochemical analyses of the sediments which indicate lateral introduction of aromatic oils and completion of organic matter maturation [6]; however, these type of analyses are extremely time consuming and less amenable to studies at high resolution. Secondly, rock magnetic analyses of Hole 1038 I indicate that diagenetic processes commence several meters above the apparent sedimentological transition from facies A to B. We suggest that rock-magnetic analyses can be used to scan sediments to identify intervals that would be interesting for analysis by other methods.

Multivariate statistical methods are of importance for visualization and interpretation of information contained in a complex rock-magnetic data set, particularly when the subtle and inherently gradual diagenetic processes are targeted.

Acknowledgements

References

[1] J. Bloemendal, J.W. Hunt, P.B. deMenocal, A. Hayashida, Origin of the sedimentary magnetic record at Ocean Drilling Program sites on the Owen Ridge, Western Arabian Sea, J. Geophys. Res. 98 (1993) 4199–4219.

[2] R. Karlin, Magnetic mineral diagenesis in sub-oxic sediments at Bettis Site W-N, NE Pacific Ocean, J. Geophys. Res. 95 (1990) 4421–4436.

[3] A.P. Roberts, Magnetic properties of sedimentary greigite (Fe_3S_4), Earth Planet. Sci. Lett. 134 (1995) 227–236.

[4] I.F. Snowball, M. Torii, Incidence and significance of ferrimagnetic iron sulphides in Quaternary studies, in: B.A. Maher, R. Thompson (Eds.), Quaternary Climates and Magnetism, Cambridge University Press, 1999.

[5] R.H. James, M.D. Rudnicki, M.R. Palmer, The alkali element and boron geochemistry of the Escanaba Trough sediment hosted hydrothermal system, Earth Planet. Sci. Lett. 171 (1999) 157–169.

[6] Shipboard Scientific Party, Escanaba Trough: sites 1037, 1038, in: Y. Fouquet, R.A. Zierenberg, D.J. Miller et al., Proc. ODP, Init. Repts., 169, College Station, TX (Ocean Drilling Program), 1998, pp. 205–297.

[7] Y. Fouquet, R.A. Zierenberg, D.J. Miller et al., Proc. ODP, Init. Repts., 169, College Station, TX (Ocean Drilling Program), 1998.

[8] A.C. Campbell, C.R. German, M.R. Palmer, T. Gamo, J.M. Edmond, Chemistry of hydrothermal fluids from the Escanaba Trough, Gorda Ridge, in: J.L. Morton, R.A. Zierenberg, C.A. Reiss (Eds.), Geologic, Hydrothermal and Biologic Studies at Escanaba Trough, Gorda Ridge, Offshore Northern California, U.S. Geological Survey Bulletin 2022, 1994, pp. 201–221.

[9] R. Zierenberg, J.L. Morton, R.A. Koski, S.L. Ross, Geologic setting of massive sulfide mineralization in the Escanaba Trough, in: J.L. Morton, R.A. Zierenberg, C.A. Reiss (Eds.), Geologic, Hydrothermal and Biologic Studies at Escanaba Trough, Gorda Ridge, Offshore Northern California, U.S. Geological Survey Bulletin 2022, 1994, pp. 171–197.

[10] C.A. Brunner, W.R. Normark, G.G. Zuffa, F. Serra, Deep-sea sedimentary record of the late Wisconsin cataclysmic floods from the Colombia River, Geology 27 (1999) 463–466.

[11] W.R. Normark, C.E. Gutmacher, R.A. Zierenberg, F.L. Wong, R.J. Rosenbauer, Sediment fill of Escanaba Trough, in: J.L. Morton, R.A. Zierenberg, C.A. Reiss (Eds.), Geologic, Hydrothermal and Biologic Studies at Escanaba Trough, Gorda Ridge, Offshore Northern California, U.S. Geological Survey Bulletin 2022, 1994, pp. 91–130.

[12] R.E. Karlin, R.A. Zierenberg, Sedimentation and neotectonism in the SESCA area, Escanaba Trough, southern Gorda Ridge, in: J.L. Morton, R.A. Zierenberg, C.A. Reiss (Eds.), Geologic, Hydrothermal and Biologic Studies at Escanaba Trough, Gorda Ridge, Offshore Northern

California, U.S. Geological Survey Bulletin 2022, 1994, pp. 131–142.

[13] T.A.T. Mullender, A.J. vanVelzen, M.J. Dekkers, Continuous drift correction and separate identification of ferrimagnetic and paramagnetic contributions in thermomagnetic runs, Geophys. J. Int. 114 (1993) 663–672.

[14] C.J. Bezdek, R. Ehrlich, W. Full, FCM the fuzzy *c*-means cluster algorithm, Comput. Geosci. 10 (1984) 191–203.

[15] S.P. Vriend, P.F. van Gaans, J. Middelburg, A. de Nijs, The application of fuzzy *c*-means cluster analysis and non-linear mapping to geochemical data sets: examples from Portugal, Appl. Geochem. 3 (1988) 213–224.

[16] M. Urbat, M.J. Dekkers, S.P. Vriend, The isolation of diagenetic groups in marine sediments using fuzzy *c*-means cluster analyses, in: D.H. Tarling, P. Turner (Eds.), Paleomagnetism and Diagenesis in Sediments, Geological Society, London, Spec. Publ. 151, 1999, pp. 85–93.

[17] M.J. Dekkers, C.G. Langereis, S.P. Vriend, P.J.M. van Santvoort, G.J. de Lange, Fuzzy *c*-means cluster analysis od early diagenetic effects on natural remanent magnetization acquisition in a 1.1 Myr piston core from the Central Mediterranean, Phys. Earth Planet. Interact. 85 (1994) 155–171.

[18] M. Urbat, M.J. Dekkers, S.P. Vriend, Fuzzy *c*-means clustering as an aid in the interpretation of the natural remanent magnetization in various types of sediments, in: V. Pawlowsky-Glahn (Ed.), Proceedings of IAMG '97, Part I, CMNE, Spain, 1997, pp. 395–400.

[19] P.P. Kruiver, Y.S. Kok, M.J. Dekkers, C.G. Langereis, C. Laj, A pseudo-Thellier relative palaeointensity record, and rock magnetic and geochemical parameters in relation to climate during the last 276 kyr in the Azores region, Geophys. J. Int. 136 (1999) 757–770.

[20] A.M. Schmidt, T. von Dobeneck, U. Bleil, Magnetic characterization of Holocene sedimentation in the South Atlantic, Paleoceanography 14 (4) (1999) 465–481.

[21] Ö. Özdemir, D.J. Dunlop, B.M. Moskowitz, The effect of oxidation on the Verwey transition in magnetite, Geophys. Res. Lett. 20 (1993) 1671–1674.

[22] M.J. Dekkers, Magnetic properties of natural pyrrhotite. II. High- and low-temperature behavior of JRS and TRM as a function of grain size, Phys. Earth Planet. Interact. 57 (1989) 266–283.

[23] P.H.M. Dankers, Magnetic properties of dispersed natural iron oxides of known grain size, Ph.D. thesis, Utrecht University, 1978.

[24] M.J. Dekkers, H.F. Passier, M.A.A. Schonnen, Magnetic properties of hydrothermally synthesized greigite (Fe_3S_4). 2. High- and low-temperature properties, Geophys. J. Int., submitted.

[25] P. Rochette, G. Fillion, L-L. Mattei, M.J. Dekkers, Magnetic transition at 30–34 K in pyrrhotite: insight into a widespread occurence of this mineral in rocks, Earth Planet. Sci. Lett. 98 (1990) 319–328.

[26] H.F. Passier, 1999, unpublished data.

[27] R. Day, M.D. Fuller, V.A. Schmidt, Hysteresis properties of titanomagnetites: grain size and composition dependence, Phys. Earth Planet. Interact. 13 (1977) 260–267.

[28] D.H. Tarling, F. Hrouda, The Magnetic Anisotropy of Rocks, Chapman and Hall, London, 1993, 217 pp.

[29] P. Rochette, M. Jackson, C. Aubourg, Rock magnetism and the interpretation of anisotropy of magnetic susceptibility, Rev. Geophys. 30 (1992) 209–226.

[30] K.S. Lackschewitz, A. Singer, R. Botz, D. Garbe-Schönberg, P. Stoffers, Mineralogical and geochemical characteristics of clay minerals in the region of the major hydrothermal site in the Escanaba Trough, Gorda Ridge, Northeast Pacific Ocean, Leg 169, Proc. ODP, 169, College Station, TX (Ocean Drilling Program), submitted.

[31] B.A. Housen, R.J. Musgrave, Rock-magnetic signature of gas hydrates in accretionary prism sediments, Earth Planet. Sci. Lett. 139 (1996) 509–519.